Journal of Magnetic Resonance 204 (2010) 219–224

Contents lists available at ScienceDirect

Journal of Magnetic Resonance

journal homepage: www.elsevier.com/locate/jmr

Enhanced sensitivity current density imaging

Igor Serša *

Jožef Stefan Institute, Jamova 39, 1000 Ljubljana, Slovenia

ARTICLE INFO

Article history:
Received 28 August 2009
Revised 24 February 2010
Available online 1 March 2010

Keywords:
Current density imaging
Sensitivity
Multi-spin–echo
Currents in electrolytes

ABSTRACT

One of the major weaknesses of current density imaging (CDI) is its poor sensitivity and therefore a need for the use of high voltage in CDI. In this work, a new CDI technique with enhanced sensitivity (ES-CDI) is presented. The ES-CDI sequence overcomes the sensitivity problem in samples with a long T_2 relaxation time that allows the use of a long current encoding period. As successful CDI detection is conditioned by a sufficiently large product of current and its application time a longer current encoding period enables the use of lower current and also lower voltage therefore significantly reducing any sample damage. In addition, the ES-CDI sequence also uses fast image signal acquisition and so enables heavy signal averaging and with it associated additional CDI sensitivity increase within the experiment time of the conventional CDI experiment. The feasibility of the ES-CDI sequence was tested on a model sample filled with physiological solution. Voltage of just 1 V and current application time of 800 ms were sufficient to detect current density of 20 A/m^2 with a detection limit of 0.7 A/m^2.

1. Introduction

Current density imaging (CDI) is an MRI technique, enabling imaging of electric current density distribution in conductive, mainly aqueous samples [1,2]. Applications of CDI range from medicine, biology, wood science to technology [3–10]. One of the major obstacles for use of CDI in medicine and biology is usually insufficient conductivity in biological samples. Unfortunately, most biological samples have also short T_2 relaxation times that pose another obstacle for successful use of CDI. These problems are not usually encountered in applications in technology, where samples are mainly electrolytic solutions, of which conductivity can be adjusted for specific experiment needs, and their T_2 relaxation times are typically an order of magnitude longer than those of biological samples. However, there are a range of CDI applications in which samples have long T_2 relaxation times, and low conductivity [11]. Here is presented a new CDI method with enhanced sensitivity, that may be a solution to these problems.

The principle of the CDI method is based on the application of currents in electric pulses that are synchronized with the imaging sequence [12]. The currents induce additional magnetic fields that add to the static magnetic field and for the time of their application cause a change of the nuclear precession frequency resulting in an accumulated phase shift. The phase shift is proportional to the time of applied currents and to the magnetic field component (of applied currents) in the direction of the static magnetic field. In the CDI experiment, the phase shifts are stored in the phase image, which is then used to obtain maps of magnetic field of applied currents. These are in the final step used to calculate a current density (CD) map using Ampere's law.

Evidently, the performance of the CDI experiment is closely associated with the magnitude of accumulated phase shifts, i.e., small phase shifts result in a noisy CD image. The magnitude of accumulated phase shifts is proportional to the product between current and the time of its application. So to improve the CDI performance current or its application time or both, have to be increased. Current can be increased by improving the sample conductivity or by applying higher voltage. The first cannot be altered in most biological samples while the second, i.e., use of high voltage, may damage samples. Often, the only alternative is the use of a longer current application time. However, this is again limited by the sample nuclear relaxation properties. Extremely long current application times may lead to a high signal loss due to the T_2 relaxation and consequently to the poor image phase determination. As this is linked with the CDI noise the result is again a noisy CD image [12–14].

In imaging sequences that use auxiliary phase encoding to encode the external event (flow, temperature, current density, ...), the encoding period is often limited not only because of sample relaxation properties, but also because its diffusion properties. This is especially true in MR microscopy experiments where imaging gradients are large. Namely, in most such sequences the first gradient is applied immediately at the beginning of the sequence (slice-selection gradient or imaging phase-encoding gradient). This is then followed by the auxiliary-encoding period that is often combined with one or more refocusing RF pulses with corresponding slice-selection gradients. The last part of the sequence is the signal

* Fax: +386 1 477 3191.
E-mail address: igor.sersa@ijs.si

1090-7807/$ - see front matter © 2010 Elsevier Inc. All rights reserved.
doi:10.1016/j.jmr.2010.02.025

acquisition part where one or more readout gradients are applied depending on the sequence (conventional spin–echo, RARE, EPI, ...). This approach, where time separation between the first (slice-selection) and the last (signal readout) gradient is large, is inevitably associated with a substantial signal loss due to diffusion, and the signal attenuation factor is approximately proportional to the third power of the time separation between the gradients and to the square of their amplitudes [15]. Elimination of the gradient use in the excitation part and in the auxiliary-encoding part of the sequence would reduce signal attenuation due to diffusion. This approach could therefore prolong the auxiliary-encoding period and increase the sensitivity of the method.

In this work a new CDI imaging sequence is presented that enables the use of current encoding periods up to 1 s in aqueous samples with long T_2 relaxation times. The long encoding period, that was achieved by the use of the train of hard refocusing RF pulses with no slice-selection gradients and with superimposed electric pulses of alternating polarity in-between the RF pulses [16,17], is combined with fast signal acquisition enabled by the two-shot RARE approach [18]. Fast signal acquisition enables many signal averages in the same experiment time as is normally needed for the conventional CDI and additionally improves the CDI sensitivity. This is because the CDI sensitivity is proportional to the signal to noise ratio (SNR) of the conventional magnitude image. Combination of both: long current encoding period and heavy signal averaging leads to enhanced sensitivity CDI (ES-CDI) that may have up to 100 times better sensitivity (current ending time is typically 40 times longer, while the additional factor of 2.5 can easily be reached by signal averaging) than the conventional CDI approach. The ES-CDI method has been theoretically analyzed and its performance verified by a series of experiments on a standard test sample.

2. Enhanced sensitivity current density imaging sequence

CDI sensitivity analysis done in Refs. [12–14] provides the following formula for the CD image noise:

$$\sigma_j = \frac{\sqrt{2}N}{\mu_0 FOV\, t_c\, SNR}, \tag{1}$$

where μ_0 is the magnetic constant, *FOV* is the imaging field of view, *N* by *N* is the image matrix size, t_c is the current application time (sum of all current pulse durations) and *SNR* is the signal to noise ratio of the conventional (signal magnitude) image. According to this formula the CDI sensitivity, i.e., the reciprocal CDI noise, is proportional to the current application time t_c and to SNR of the conventional image. However, t_c and *SNR* are not independent. In the conventional CDI sequence, i.e., the DC-CDI sequence (Fig. 1a), t_c approximately corresponds to the spin–echo time of the sequence so that *SNR* is proportional to $\exp(-t_c/T_2)$ and therefore the CDI sensitivity is proportional to $t_c \exp(-t_c/T_2)$. Obviously, the CDI sensitivity limit is zero in both t_c extremes (very short or very long t_c) and reaches maximum at $t_c = T_2$. In reality, the optimal t_c depends on diffusion and susceptibility effects, and is shorter than the T_2 relaxation time of the sample. The CDI sensitivity can be at a given t_c further increased also by increasing *SNR* with signal averaging.

The DC-CDI sequence (Fig. 1a) is based on the standard 2D spin–echo imaging sequence to which two electric pulses of opposite polarity are added [1]. The DC-CDI sequence is designed for CDI with t_c of the order of 10–100 ms. However, this criterion is met at a moderate voltage of electric pulses (of the order of 10 V) only for electrolytic samples with significantly higher conductivity than is typical for biological samples. To image current density at moderate voltage in samples with low conductivity, t_c must be prolonged to several 100 ms. For such long t_c values the DC-CDI sequence fails because either, the T_2 relaxation time may not be

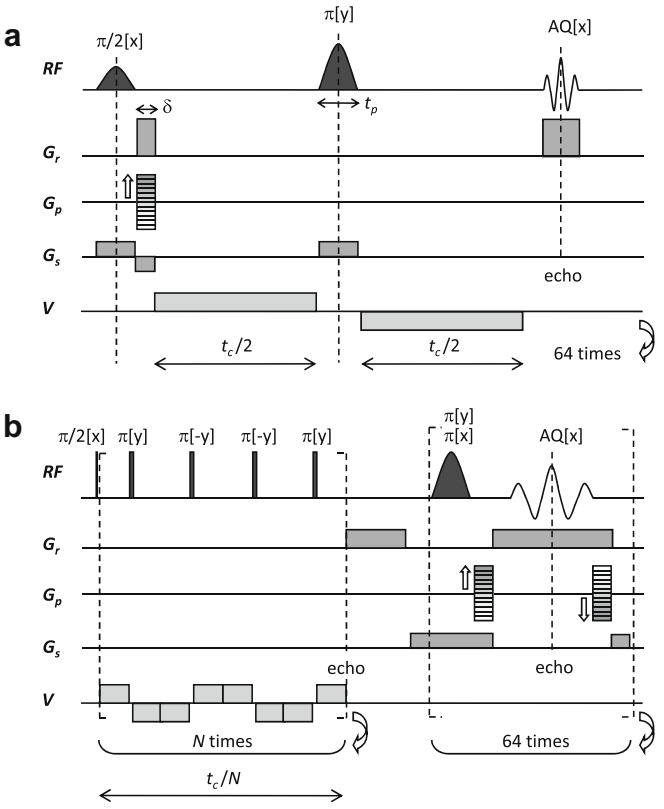

Fig. 1. Two CDI sequences: (a) conventional CDI (DC-CDI) sequence and (b) enhanced sensitivity CDI (ES-CDI) sequence with optimized performance for samples with long T_2 relaxation time and fast diffusion. The DC-CDI sequences are based on the standard 2D spin–echo sequence to which are added two electric pulses of opposite polarity. The ES-CDI sequence consists of two parts; the first current encoding part and the second, fast image signal acquisition part. The current encoding part uses a train of hard refocusing RF pulses with the MLEV-4 phase cycling that are superimposed to electric pulses of alternating polarity, while the image acquisition part is based on the two-shot RARE image signal acquisition.

long enough (mainly in biological samples), or fast diffusion causes signal attenuation that is associated with the use of imaging gradients (mainly in electrolytic samples). An estimate for the signal attenuation due to diffusion may be obtained using Stejskal–Tanner formula [15]:

$$S = S_0 \exp(-D\gamma^2 G_r^2 \delta^2 (t_c + t_p + 2/3\delta)). \tag{2}$$

Here S_0 is the image signal assuming diffusion is zero, *D* is the apparent diffusion coefficient, γ is the gyromagnetic ratio, t_p is the refocusing pulse width, G_r is the image readout gradient amplitude and δ is its application time (Fig. 1a). It is also assumed that phase and slice imaging gradients have lesser effect on signal attenuation. As follows from Eq. (2) the attenuation exponent is proportional to the apparent diffusion coefficient, to the current application time and to the readout gradient amplitude squared. As the readout gradient amplitude is inversely proportional to the imaging field of view:

$$G_r = \frac{2\pi}{\gamma\, DW\, FOV} \tag{3}$$

(here DW is the signal acquisition dwell time), the signal attenuation increases with increasing image resolution. In addition to the diffusion signal attenuation in the DC-CDI sequence, at long current encoding times the signal attenuates also due to T_2^* relaxation that is associated with internal gradients in the sample.

The ES-CDI sequence (Fig. 1b) is optimized for long current encoding periods, enabled by reduction of diffusion and T_2^* effects on the signal attenuation, as well as for fast signal acquisition. It

consists of two parts. The first (current encoding part) is designed to enable long current encoding periods in samples with a long T_2 relaxation time and fast diffusion. This is accomplished by the use of the train of hard refocusing RF pulses between which electric pulses of alternating polarity are applied. Use of a dense train of refocusing RF pulses significantly reduces the signal attenuation due to diffusion as well as susceptibility effects and with them associated T_2^* relaxation. The diffusion signal attenuation is further reduced by exclusion of imaging magnetic field gradients in the current encoding part of the sequence so that the signal decays with the T_2 relaxation rate. The polarity of electric pulses is changed after each refocusing RF pulse in order to sum phase shifts accumulated during individual electric pluses [16,17]. Namely, each refocusing RF pulse reverses the magnetization phase. The stability of the sequence was improved by the use of MLEV-4 phase cycling of refocusing RF pulses [19].

The second part of the ES-CDI sequence is the image signal acquisition part, which is based on the two-shot RARE approach [18]. The conventional RARE method [20], that uses the CPMG train of refocusing RF pulses $\pi[y]$, can refocus magnetization following the excitation RF pulse $\pi/2[x]$, while it cannot refocus magnetization following the excitation RF pulse $\pi/2[y]$; this "off phase" magnetization component can be refocused by the CPMG train of refocusing RF pulses $\pi[x]$. As in ES-CDI such "off phase" magnetization components are created by electric currents the conventional RARE method are inconvenient for the image signal acquisition. The solution is to use two RARE sequences that have phases of refocusing RF pulses 90° apart (CPMG trains of refocusing RF pulses $\pi[x]$ and $\pi[y]$) of which signals are combined, i.e., the two-shot RARE approach. Each of the sequences preserves a signal of one of the two perpendicular initial magnetization components, while their sum preserves the entire signal. With fast image signal acquisition, many signal averages can be done in the same experiment time as is normally needed for the conventional CDI experiment. As it is evident from Eq. (1), signal averaging, that improves SNR with the square root of signal averages, can also significantly contribute to higher CDI sensitivity.

3. Materials and methods

Electric pulses of the ES-CDI sequence generate currents through the sample that produce additional magnetic field B_c in the sample. The magnetic field adds to the static magnetic field and temporarily changes the nuclear precession frequency, which results in a phase shift φ that is proportional to the component of magnetic field change in the direction of the static magnetic field B_{c_z} and to the time of current application t_c:

$$\varphi = \gamma B_{c\_z} t_c. \tag{4}$$

Relation in Eq. (4) enables calculation of B_{c_z} from the measured image of phase shifts φ and from known t_c. In general all three components of B_c must be known so that current density can be calculated using the Ampere's law:

$$\vec{j} = \frac{1}{\mu_0} \nabla \times \vec{B_c}. \tag{5}$$

Often, current direction is known but not its distribution. Suppose that the current direction is z so that for its calculation two components of the magnetic field change (B_{c_x} and B_{c_y}) must be known:

$$j_z = \frac{1}{\mu_0}\left(\frac{\partial B_{c\_x}}{\partial y} - \frac{\partial B_{c\_y}}{\partial x}\right). \tag{6}$$

The two components of the magnetic field change can be measured in two perpendicular sample orientations, such that the coordinate system that rotates with the sample is once rotated to orientation with the x-axis parallel with the static magnetic field (to measure B_{c_x}) and then to orientation with the y-axis parallel with the static magnetic field (to measure B_{c_y}). In few cases the sample rotation to acquire magnetic field change maps in two perpendicular orientations can be avoided. One of these is a sample with a cylindrical symmetry and therefore with cylindrically symmetric current distribution that was also used as a test sample for testing sensitivity of the ES-CDI sequence (Fig. 2). In CDI experiments current was flowing along the sample symmetry axis and the current density was imaged in a plane perpendicular to the current direction. For the sample, the two magnetic field change maps acquired in two orientations 90° apart around the symmetry axis would be identical due to the sample symmetry. Therefore, the magnetic field change map (B_{c_x}) was acquired in only one orientation and the second map (B_{c_y}) was simply copied from the first map (B_{c_x}). Finally, current density was calculated from B_{c_x} and B_{c_y} maps using Eq. (6).

The cylindrical test sample consisted of two concentric 13 mm long cylindrical tubes that were filled to the top with physiological solution (0.9% saline) with relaxation times T_1 = 2870 ± 70 ms and T_2 = 1930 ± 10 ms (measured at 2.35 T). An inner tube with a diameter of 4 mm, was closed and sealed at both ends with copper electrodes that were connected to a voltage amplifier which generated electric pulses with an adjustable voltage. To prevent any contribution of the magnetic field of return wires to the calculated current density the return wires were perfectly aligned with the direction of the static magnetic field (Fig. 1). The return wires generated magnetic fields $B_{w\_x}(x, z)$ and $B_{w\_z}(x, z)$, which were canceled in calculation of current density using Eq. (6), i.e., $\partial B_{w\_x}(x,z)/\partial y = 0$. The pulses were triggered by TTL signals from the spectrometer. In the experiments electric pulses of 1 V were used so that uniform current of an amplitude 200 μA was flowing along the inner tube. The outer tube with the diameter of 10 mm was used as a reference and was not connected to the voltage supply so that no current was flowing through it.

Two different CDI sequences were tested: the DC-CDI sequence (Fig. 1a) and the ES-CDI sequence (Fig. 1b). The DC-CDI sequence was tested with no signal averaging at total current application time of t_c = 20 ms (two 10 ms electric pulses) and t_c = 800 ms (two 400 ms electric pulses), while the ES-CDI was tested at t_c = 800 ms without signal averaging and with 10 signal averages. The current encoding part of the ES-CDI sequence consisted of N = 5 blocks of eight 20 ms long electric pulses. In all experiments imaging parameters were identical: imaging field of view 15 mm, slice thickness 2 mm, image matrix 64 by 64, acquisition bandwidth 50 kHz (dwell time 10 μs) and slice orientation transversal to the cylinder axis of the sample. Echo time and repetition time of the DC-CDI sequence were: TE/TR = 23/1024 ms and TE/TR = 823/1824 ms for the experiments with t_c = 20 ms and t_c = 800 ms, respectively, while image acquisition parameters for the ES-CDI sequence were the following: number of echoes 64, gra-

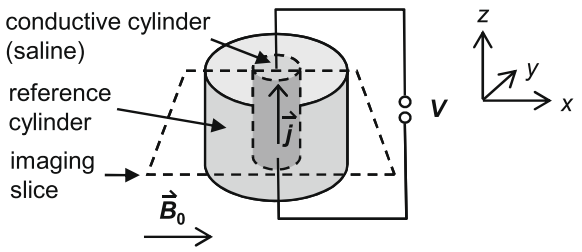

Fig. 2. The standard test sample for CDI experiments consists of two concentric tubes; the inner one (with electrodes at both ends) through which current flows and the outer reference tube. Both tubes were filled with physiological solution (0.9% saline). The imaging slice was perpendicular to the cylinder axis.

dient readout time 1140 μs (including 250 μs gradient raise time and another 250 μs gradient fall time), inter-echo time 2640 μs and repetition time TR = 10,970 ms. Long TR of more than $3T_1$ was needed to ensure an identical fully relaxed initial magnetization in both steps of the two-shot RARE acquisition used in the ES-CDI sequence. Total imaging time was 70 s in the DC-CDI experiments and was 22 and 220 s in the ES-CDI experiment with no averaging and with 10 averages, respectively.

Experiments were performed on a 2.35 T horizontal bore Oxford (Oxon, UK) superconducting magnet connected to a TecMag (Houston, Texas, USA) Apollo spectrometer equipped with Bruker (Ettlingen, Germany) micro-imaging accessories. To prevent RF disturbances from external RF sources, all electric cable connections between the sample and the voltage amplifier were filtered by low-pass RF filters mounted on the RF cage surrounding the magnet.

CD images were calculated using our own C-code written software implementing the above described CDI calculation procedure based on Eqs. (4) and (6). All other image processing, i.e., image SNR analysis and image histograms, was done by the ImageJ program (National Institute of Health, Bethesda, Maryland, USA).

4. Results

Results of four different CDI experiments (DC-CDI at t_c = 20 ms and t_c = 800 ms and ES-CDI experiments at t_c = 800 ms without and with 10 averages) on the cylindrical test sample are presented in Fig. 3 with magnitude (a, e, i, and m), real signal component (b, f, j, and n), calculated CD images (c, g, k, and o) and current density distribution histograms (d, h, l, and p). It can clearly be seen that the conventional CDI method (DC-CDI) yields a strong signal at a standard current encoding time of t_c = 20 ms (2 × 10 ms), which results in a good SNR magnitude image. (Fig. 3a). As the sample had low conductivity, the current encoding time was too short to encode a large enough phase shift in the signal phase so that the calculated CD image that displays current in the range −6 to 30 mA is very noisy and shows no evidence of current in the inner cylinder of the sample (Fig. 3c). In the next DC-CDI experiment the current encoding time of t_c = 800 ms (2 × 400 ms) was long enough to encode enough phase shift in the signal phase and the corresponding calculated CD image shows a presence of current in the inner cylinder of the sample. However, the calculated CD image is very noisy due to the excessively long current encoding period and with it associated poor SNR of the corresponding magnitude image (Fig. 3e). In addition the image has a non-uniform signal distribution and a significant signal loss in the proximity of sample interfaces.

The ES-CDI method (40 × 20 ms) has significantly less artefacts despite the long current encoding time of t_c = 800 ms. The magnitude image (Fig. 3i) is uniform and sample interfaces have no signal loss. The real signal component image of the ES-CDI method (Fig. 3j) has more regular pattern of interchanging dark and bright bands than the real signal component image of the corresponding conventional CDI method (Fig. 3f), which indicates more accurate phase shift accumulation in the case of the ES-CDI method. The corresponding CD image (Fig. 3k) has relatively low image noise

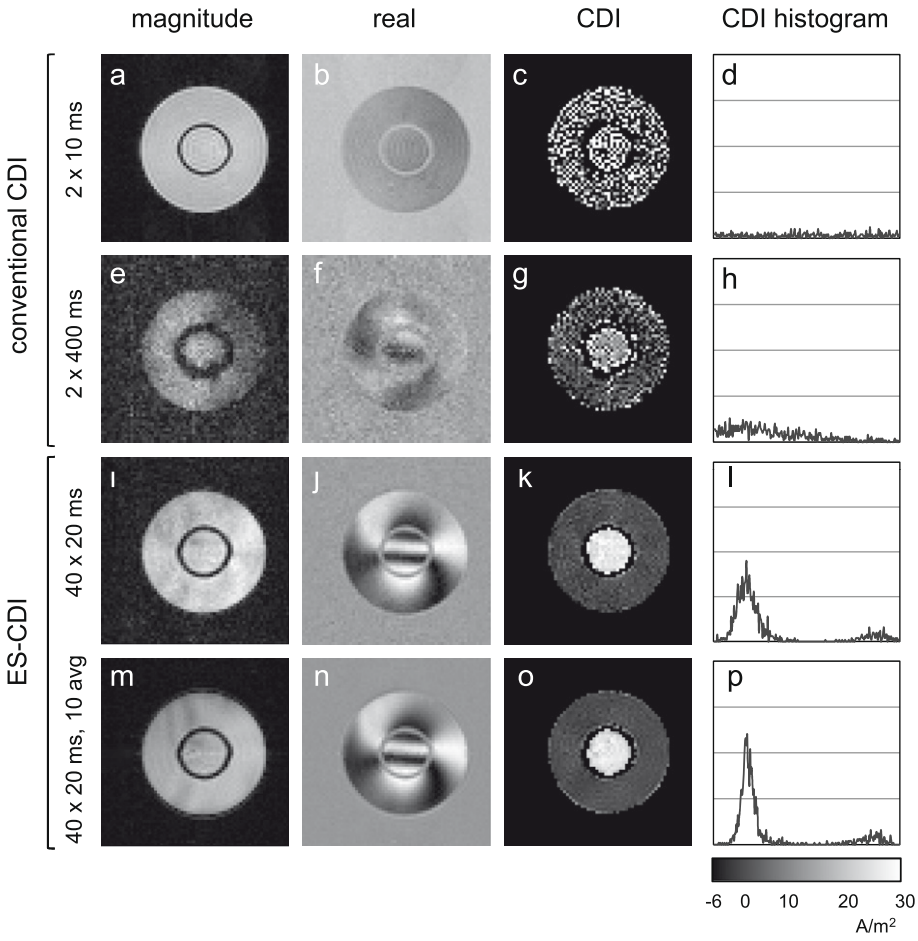

Fig. 3. Results of the conventional CDI experiment with short (2 × 10 ms; a–d) and long (2 × 400 ms; e–h) current pulses and the ES-CDI experiment without (40 × 20 ms; i–l) and with (40 × 20 ms, 10 avg.; m–p) signal averaging presented by magnitude (a, e, i, and m), real signal component (b, f, j, and n) and calculated current density (c, g, k, and o) images as well as with image brightness histograms of current density images (d, h, l, and p).

and clearly delineated current region corresponding to the inner tube region. The current distribution is more uniform than in the CD image of the corresponding conventional CDI method (Fig. 3g). The best results were obtained with the ES-CDI method with signal averaging (40 × 20 ms, 10 avg.). The result of averaging (10 repetitions were used) is highly increased SNR in the magnitude image (Fig. 3m) as well as in real and imaginary images (Fig. 3n). Measured SNRs in magnitude images of the ES-CDI method with no averaging in Fig. 3i and the ES-CDI method with averaging in Fig. 3m are 19 and 50, respectively. Due to the increased SNRs of both real and imaginary signal component images the signal phase is more accurate and so is the CD image calculated from the signal phase accumulated during the application of electric current. The CD image in Fig. 3o obtained using ES-CDI with signal averaging shows identical current density in the inner tube as the ES-CDI method without averaging in Fig. 3k (23.8 A/m^2 vs. 24.6 A/m^2), however, current density noise was significantly lower in the ES-CDI experiment with averaging (0.7 A/m^2 vs. 1.5 A/m^2).

Current distribution in the sample can be analyzed also by histograms of current density distribution (Fig. 3d, h, l, and p). The histogram of conventional CDI (2 × 10 ms) in Fig. 3d shows almost uniform current noise through the entire sample. The histogram integral is also reduced as many points had current out of the displayed range. Slight indication of current distribution is evident in the histogram of conventional CDI (2 × 400 ms) in Fig. 3h that shows a prevalence of zero current over the inner tube current at 24 A/m^2. A peak, corresponding to current in the inner tube, is due to excessive noise being practically undetectable. In the case of the ES-CDI method (40 × 20 ms, Fig. 3l), two peaks, the bigger corresponding to zero current in the outer tube, and the smaller corresponding to the current in the inner tube, are clearly visible. The narrowest peaks, i.e., the lowest CDI noise, were obtained in the histogram corresponding to the ES-DCI experiment with signal averaging (40 × 20 ms, 10 avg.; Fig. 3p). The ratio between histogram peak widths for CDI experiments 2 × 400 ms, 40 × 20 ms, and 40 × 20 ms, 10 avg. is approximately 4:2:1.

5. Discussion

Successful detection of current density by CDI sequences is conditioned by a large enough magnetization phase shift produced by an additional magnetic field induced by the current flowing through a conductive sample. The phase shift is proportional to the current amplitude and to the time of its application, i.e., to the current encoding period. In conventional CDI sequences (DC-CDI, AC-CDI, DC-AC-CDI) [16] the current encoding period is relatively short and normally does not exceed a few tens of milliseconds. Therefore, to obtain a large enough phase shift, the short current encoding period has to be compensated by larger current amplitude. This is in a typical MR microscopy experiment, where the sample size is typically a centimeter in diameter, of the order of few 10 mA, which corresponds to a typical current density of a few 1000 A/m^2. This current density is easily attainable using moderate voltage with artificially made electrolytic samples of which conductivity can be adjusted for the needs of the experiment. In some cases, the sample may still have relatively long T_2 relaxation time, however, low conductivity which cannot be altered [11]. For these cases ES-CDI may be the right choice.

The ES-CDI approach significantly reduces problems associated with the use of CDI in samples with long T_2 relaxation times, and fast diffusion. As the current encoding period in the ES-CDI sequence is up to 50 times longer than in the conventional CDI sequence, the current amplitude and therefore, also the applied voltage may be up to 50 times lower in the ES-CDI sequence compared to the conventional CDI sequence. Instead of using up to several hundred volts for electric pulses in the conventional CDI experiment (as evident from Eq. (1) the need for a higher voltage is increasing with an increasing CDI resolution) use of electric pulses with a voltage of less than 10 V is sufficient in the ES-CDI experiment. In the presented ES-CDI experiment in Fig. 3, the test sample was filled with physiological solution (0.9% saline) and the applied voltage was only 1 V. The dissipated energy in the sample due to its electrical resistance is proportional to the square of the applied voltage and the time of its application. Therefore 50-fold voltage reduction results in 2500-times lower dissipated electric power and 50 times lower dissipated energy (due to 50 times longer current encoding period).

The sensitivity improvement of the ES-CDI sequence is enabled by the use of a long current encoding period and fast image signal acquisition allowing heavy signal averaging within a reasonable experimental time. Advantages of a long current encoding period are apparent, and were successfully verified experimentally, however, the signal averaging yielded images of lower SNR than theoretically expected .In theory, 10 signal averages should yield $\sqrt{10}$ = 3.2-fold SNR improvement of the conventional magnitude image and the same SNR improvement also in the corresponding CD image. The SNR improvement between experiments with and without signal averaging was equal to 50/19 = 2.6 in corresponding magnitude images and was equal to 34/16 = 2.1 in corresponding CD images. More detailed analysis showed that the signal after averaging was, as expected, 10 times larger, while the noise increase was approximately 3.8-fold instead of the expected 3.2-fold. The discrepancy can be attributed to the systematic background noise-like signals due to the MR hardware imperfections such as B_0, shim or gradient instability. As the instrumentation noise increases as a regular signal, i.e., with the number of averages and the random noise increases with the square root of the number of averages, then, for each experiment there exists a critical number of averages beyond which signal averaging does not further improve image SNR.

Often, heavy averaging of a signal from a single slice is not the optimal choice. This is especially true in cases where signal acquisition from neighboring slices is needed. In these cases use of the 3D RARE sequence with phase encoding in the slice direction and with hard instead of adiabatic refocusing RF pulses is a better choice than the 2D RARE sequence with averaging of the signal from the selected slice. Interestingly, in a given experiment time, both approaches are equivalent in terms of the SNR increase compared to the single slice 2D experiment with no averaging, i.e., the increase in the 2D experiment with N averages is equal to the factor $\sqrt{N}$, while the increase in the 3D experiment with M phase encoding steps and N/M averages is equal to the product of factors $\sqrt{M}$ (due to parallel signal acquisition in imaging with phase encoding) and $\sqrt{N/M}$ (due to signal averaging). However, a major difference between the experiments is that in the same experiment time in the 3D experiment the signal is acquired from the entire sample while in the 2D experiment it is acquired only from a single slice.

In biological samples, the sample conductivity is usually much lower than in artificially made electrolytic samples so that the current density of electrolytic samples can only be obtained by the use of high voltage; typically of several 100 V. This may often result in tissue damage, especially if the image signal is acquired in a standard manner that requires as many signal excitations and current encoding periods as there are image lines. Application of high voltage in *in vivo* experiments can cause severe pain and can only be done under anesthesia and with a very limited number of repeated electric pulses, i.e., only by using CDI with rapid image acquisition. The tissue damage problem can be avoided by the use of lower voltage in CDI. However, this is associated with an increase of the current encoding period for the factor of the voltage decrease.

Unfortunately, most biological samples have short T_2 relaxation times that usually do not exceed 100 ms. This poses a hard restriction on the use of long current encoding periods in such systems, i.e., to attain a good quality CD image the current encoding period (t_c) should in principle not exceed the T_2 relaxation time of the sample. The condition poses a hard restriction on t_c and makes the ES-CDI performance in most biological samples equal to that of the conventional CDI (DC-CDI); ES-CDI advantages such as reduced effects of diffusion and reduced internal gradient and susceptibility effects are diminished. Obviously, in biological systems CDI cannot be performed without the use of sufficiently high voltage. From that perspective, fast signal acquisition, enabled by the ES-CDI sequence, is especially important as it helps reducing the number of applied electric pulses and with them associated tissue damage.

The other problem, which is common to all CDI sequences except the RF-CDI [21], is a need for sample rotation to perpendicular orientations in order to measure different spatial components of magnetic field change maps. However, even a real signal component image measured in just one sample orientation may to some extent give a hint on a possible current density distribution [5]. In addition, magnetic resonance electrical impedance tomography (MREIT), which is an extension of CDI, is also based on data acquisition with only one sample orientation [22].

Probably the greatest challenge of CDI is a direct neuronal current detection [23–25]. Neuronal currents flow along axons in nerve impulses (action potentials), which typically last for 1 ms. The magnetic field next to an axon during a nerve impulse is typically of the order of 100 pT [23], which yields for an axon with 20 μm diameter 5 nA neuronal current and 16 A/m^2 neuronal current density. In the presented ES-CDI experiment the current amplitude was 200 μA which is still several orders of magnitude more than the neuronal current, however, the corresponding current density of 24 A/m^2 is practically identical to the current density flowing along axons in nerve impulses. Therefore, a problem of successful nerve current detection is not only a short T_2 relaxation time problem, but also a resolution problem, i.e., how to cover the axon cross-section with sufficient pixels having good SNR. T_2 relaxation times of brain at 1 T are: 92 ms (gray matter) and 101 ms (white matter) [26], while the only brain component with long enough T_2 to enable ES-CDI is cerebrospinal fluid with relaxation times comparable to that of water. In addition, a single nerve impulse with millisecond duration would not produce a large enough phase shift. Therefore, within the current encoding period, several hundred nerve impulses would need to be triggered. As the frequency of the impulses is limited to approximately 100 Hz, due to the nerve refractory period, the effective nerve current application time reduces to approximately 100 ms. Another difficulty is associated with the unipolarity of nerve impulses so that in the ES-CDI sequence the nerve impulses can be triggered in the current encoding period only after every other refocusing RF pulse.

6. Conclusion

The presented ES-CDI sequence enables imaging of much lower current densities than other conventional CDI methods (typically of the order of 10 A/m^2 vs. 1000 A/m^2). The 100-fold sensitivity increase is enabled by the use of a long current encoding period and signal averaging. These two are attained by the elimination of imaging gradients in the current encoding period and the use of fast image signal acquisition. The increased sensitivity has a potential to widen the scope of ES-CDI applications to samples with long T_2 relation times in which low sample conductivity and with it, the associated need of high-voltage electric pulses were the limiting factor.

Acknowledgments

The author thanks to Jernej Vidmar for many fruitful discussions and to Peter Ryan for proofreading the manuscript.

References

[1] M. Joy, G. Scott, M. Henkelman, In vivo detection of applied electric currents by magnetic resonance imaging, Magn. Reson. Imaging 7 (1989) 89–94.
[2] G.C. Scott, M.G. Joy, R.L. Armstrong, R.M. Henkelman, Measurement of nonuniform current density by magnetic resonance, IEEE Trans. Med. Imaging 10 (1991) 362–374.
[3] R.S. Yoon, T.P. DeMonte, K.F. Hasanov, D.B. Jorgenson, M.L. Joy, Measurement of thoracic current flow in pigs for the study of defibrillation and cardioversion, IEEE Trans. Biomed. Eng. 50 (2003) 1167–1173.
[4] R.S. Yoon, A. Czaya, H.C. Kwan, M.L. Joy, Changes in the complex permittivity during spreading depression in rat cortex, IEEE Trans. Biomed. Eng. 46 (1999) 1330–1338.
[5] I. Sersa, K. Beravs, N.J. Dodd, S. Zhao, D. Miklavcic, F. Demsar, Electric current density imaging of mice tumors, Magn. Reson. Med. 37 (1997) 404–409.
[6] K. Beravs, D. White, I. Sersa, F. Demsar, Electric current density imaging of bone by MRI, Magn. Reson. Imaging 15 (1997) 909–915.
[7] K. Beravs, P. Oven, I. Serša, N. Torelli, F. Demšar, Electric current density imaging of pedunculate oak (*Quercus robur* L.) twigs by magnetic resonance imaging, Holzforschung 52 (1998) 541–545.
[8] B. Buhai, T. Binser, R. Kimmich, Electroosmotic flow, ionic currents, and pressure-induced flow in microsystem channel networks: NMR mapping and computational fluid dynamics simulations, Appl. Magn. Reson. 32 (2007) 25–49.
[9] B. Buhai, R. Kimmich, Dissimilar electro-osmotic flow and ionic current recirculation patterns in porous media detected by NMR mapping experiments, Phys. Rev. Lett. 96 (2006) 174501.
[10] E. Kossel, M. Weber, R. Kimmich, Visualization of transport: NMR microscopy experiments with model objects for porous media with pore sizes down to 50 micron, Solid State Nucl. Magn. Reson. 25 (2004) 28–34.
[11] O.F. Tower, The Conductivity of Liquids; Methods, Results, Chemical Applications and Theoretical Considerations, Chemical Pub. Co., Easton, PA, 1905.
[12] G.C. Scott, M.L.G. Joy, R.L. Armstrong, R.M. Henkelman, Sensitivity of magnetic-resonance current-density imaging, J. Magn. Reson. 97 (1992) 235–254.
[13] I. Sersa, O. Jarh, F. Demsar, Magnetic resonance microscopy of electric currents, J. Magn. Reson. A111 (1994) 93–99.
[14] G.C. Scott, NMR Imaging of Current Density and Magnetic Fields, Ph.D. thesis, University of Toronto, 1993.
[15] E.O. Stejskal, J.E. Tanner, Spin diffusion measurements: spin echoes in the presence of a time-dependent field gradient, J. Chem. Phys. 42 (1965) 288–292.
[16] I. Sersa, Current density imaging sequences with separation of mobile-ion current from immobile-ion current, J. Magn. Reson. 196 (2009) 33–38.
[17] U. Mikac, F. Demsar, K. Beravs, I. Sersa, Magnetic resonance imaging of alternating electric currents, Magn. Reson. Imaging 19 (2001) 845–886.
[18] I. Sersa, Auxiliary phase encoding in multi spin–echo sequences: application to rapid current density imaging, J. Magn. Reson. 190 (2008) 86–94.
[19] T. Gullion, D.B. Baker, M.S. Conradi, New, compensated Carr-Purcell sequences, J. Magn. Reson. 89 (1990) 479–484.
[20] J. Hennig, A. Nauerth, H. Friedburg, RARE imaging: a fast imaging method for clinical MR, Magn. Reson. Med. 3 (1986) 823–883.
[21] G.C. Scott, M.L. Joy, R.L. Armstrong, R.M. Henkelman, RF current density imaging in homogeneous media, Magn. Reson. Med. 28 (1992) 186–201.
[22] O. Kwon, E.J. Woo, J.R. Yoon, J.K. Seo, Magnetic resonance electrical impedance tomography (MREIT): simulation study of J-substitution algorithm, IEEE Trans. Biomed. Eng. 49 (2002) 160–167.
[23] G.E. Hagberg, M. Bianciardi, B. Maraviglia, Challenges for detection of neuronal currents by MRI, Magn. Reson. Imaging 24 (2006) 483–493.
[24] A.M. Cassara, B. Maraviglia, S. Hartwig, L. Trahms, M. Burghoff, Neuronal current detection with low-field magnetic resonance. simulations and methods, Magn. Reson. Imaging 27 (2009) 1131–1139.
[25] R.S. Wijesinghe, B.J. Roth, Detection of peripheral nerve and skeletal muscle action currents using magnetic resonance imaging, Ann. Biomed. Eng. 37 (2009) 2402–2406.
[26] P.A. Bottomley, T.H. Foster, R.E. Argersinger, L.M. Pfeifer, A review of normal tissue hydrogen NMR relaxation times and relaxation mechanisms from 1–100 MHz: dependence on tissue type, NMR frequency, temperature, species, excision, and age, Med. Phys. 11 (1984) 425–448.